1-18-2022

Phage-Encoded Cationic Antimicrobial Peptide Required for Lysis

Ashley Holt
Texas A & M University - College Station

Jesse Cahill
Texas A & M University - College Station

Jolene Ramsey
Texas A & M University - College Station

Cody Martin
Texas A & M University - College Station

Chandler O'Leary
Texas A & M University - College Station

See next page for additional authors

Recommended Citation

Holt A, Cahill J, Ramsey J, Martin C, O'Leary C, Moreland R, Maddox LT, Galbadage T, Sharan R, Sule P, Cirillo JD, Young R. 2022. Phage-encoded cationic antimicrobial peptide required for lysis. J Bacteriol 204:e00214-21. https://doi.org/10.1128/JB.00214-21.

AMERICAN SOCIETY FOR MICROBIOLOGY | Journal of Bacteriology®

MEETING PRESENTATION

Phage-Encoded Cationic Antimicrobial Peptide Required for Lysis

Ashley Holt,[a,b*] Jesse Cahill,[a,b*] Jolene Ramsey,[a,b] Cody Martin,[a,b] Chandler O'Leary,[a,b*] Russell Moreland,[a,b*] Lori T. Maddox,[a,b] Thushara Galbadage,[c*] Riti Sharan,[c*] Preeti Sule,[c*] Jeffrey D. Cirillo,[c] Ry Young[a,b]

[a]Center for Phage Technology, Texas A&M University, College Station, Texas, USA
[b]Department of Biochemistry and Biophysics, Texas A&M University, College Station, Texas, USA
[c]Department of Microbial Pathogenesis and Immunology, Texas A&M University Health, Bryan, Texas, USA

Ashley Holt, Jesse Cahill, and Jolene Ramsey contributed equally to this work. First-author order reflects the chronological order of participation in the project.

ABSTRACT Most phages of Gram-negative bacteria hosts encode spanins for disruption of the outer membrane, which is the last step in host lysis. However, bioinformatic analysis indicates that ~15% of these phages lack a spanin gene, suggesting they have an alternate way of disrupting the outer membrane (OM). Here, we show that the T7-like coliphage phiKT causes an explosive cell lysis associated with spanin activity despite not encoding spanins. A putative lysis cassette cloned from the phiKT late gene region includes the hypothetical novel gene 28 located between the holin and endolysin genes and supports inducible lysis in *Escherichia coli* K-12. Moreover, induction of an isogenic construct lacking gene 28 resulted in divalent cation-stabilized spherical cells rather than lysis, implicating gp28 in OM disruption. Additionally, gp28 was shown to complement the lysis defect of a spanin-null λ lysogen. Gene 28 encodes a 56-amino acid cationic protein with predicted amphipathic helical structure and is membrane-associated after lysis. Urea and KCl washes did not release gp28 from the particulate, suggesting a strong hydrophobic membrane interaction. Fluorescence microscopy supports membrane localization of the gp28 protein before lysis. The protein gp28 is similar in size, charge, predicted fold, and membrane association to the human cathelicidin antimicrobial peptide LL-37. Synthesized gp28 behaved similarly to LL-37 in standard assays mixing peptide and cells to measure bactericidal and inhibitory effects. Taken together, these results indicate that phiKT gp28 is a phage-encoded cationic antimicrobial peptide that disrupts bacterial outer membranes during host lysis and, thus, establishes a new class of phage lysis proteins, the disruptins.

IMPORTANCE We provide evidence that phiKT produces an antimicrobial peptide for outer membrane disruption during lysis. This protein, designated a disruptin, is a new paradigm for phage lysis and has no similarities to other known lysis genes. Although many mechanisms have been proposed for the function of antimicrobial peptides, there is no consensus on the molecular basis of membrane disruption. Additionally, there is no established genetic system to support such studies. Therefore, the phiKT disruptin may represent the first genetically tractable antimicrobial peptide, facilitating mechanistic analyses.

KEYWORDS antimicrobial peptides, bacteriophage lysis, bacteriophages, disruptin, outer membrane, small proteins

As reviewed recently by Cahill and Young 2019 (1), lysis of Gram-negative bacteria hosts requires three classes of phage proteins, each targeting one layer of the cell envelope: holins for the inner membrane (IM), endolysins for the cell wall/peptidoglycan (PG), and spanins for the outer membrane (OM) (1). In phage lambda, these proteins are encoded by four genes. *S* encodes the holin, *R* encodes the endolysin, and the nested genes

Citation Holt A, Cahill J, Ramsey J, Martin C, O'Leary C, Moreland R, Maddox LT, Galbadage T, Sharan R, Sule P, Cirillo JD, Young R. 2022. Phage-encoded cationic antimicrobial peptide required for lysis. J Bacteriol 204:e00214-21. https://doi.org/10.1128/JB.00214-21.

Editor Tina M. Henkin, Ohio State University

Address correspondence to Ry Young, ryland@tamu.edu.

*Present address: Ashley Holt, University of Wisconsin—Madison, School of Medicine and Public Health, Madison, Wisconsin, USA; Jesse Cahill, Sandia National Laboratories, Albuquerque, New Mexico, USA; Chandler O'Leary, Health Science Center, University of North Texas, Fort Worth, Texas, USA; Russell Moreland, School of Medicine, The University of Texas Rio Grande Valley, Edinburg, Texas, USA; Thushara Galbadage, Department of Kinesiology and Health Science, Biola University, La Mirada, California, USA; Riti Sharan Southwest National Primate Research Center, Texas Biomedical Research Institute, San Antonio, Texas, USA; Preeti Sule, Sanofi Pasteur, Garner, North Carolina, USA.

Received 3 May 2021
Accepted 23 July 2021
Accepted manuscript posted online 2 August 2021
Published 18 January 2022

Rz/*Rz1* encode the two spanin subunits, the IM protein Rz and the OM lipoprotein Rz1 (Fig. 1A). Lysis is initiated by the sudden formation of micrometer-scale holes in the IM by the holin (Fig. 1B). These massive, nonspecific holes allow the endolysin to escape to the periplasm and attack the PG. A second type of lysis system used by many phages was originally found in the lambdoid phage 21, which has a pinholin (S^{21}) and a signal-arrest-release (SAR) endolysin (R^{21}). The lambdoid phage 21 pinholin forms heptameric "pinholes" with ~2 nm pores. Pinholins require SAR endolysins, muralytic enzymes with N-terminal SAR domains. The SAR domain causes the enzyme to be exported by the host translocon to the periplasm, where it accumulates in a membrane-tethered, enzymatically inactive form. When the pinholins form the pinholes, the IM is depolarized, causing the SAR endolysin to be released from the bilayer and refolded into a muralytically active form.

Despite the drastically different mechanisms, the canonical holin endolysin and pinholin-SAR endolysin systems both result in temporally scheduled, enzymatic degradation of the PG. In lambda, the next and final step is disruption of the OM by the spanins, which is a periplasm-spanning heterotetrameric complex consisting of two copies each of Rz and Rz1 (2). A model for the disruption of the OM by the spanins has recently been proposed and is based on similarities with eukaryotic viral fusion proteins (3). PG degradation initiates the last step in lysis where the spanin complex is thought to undergo oligomerization and a major conformational change, resulting in fusion of the IM and OM. Some phages, including the classic coliphage T1, encode unimolecular spanins that have both an OM lipoprotein signal and a C-terminal TMD in the same gene product. These "u-spanins", which connect the IM and OM, are also thought to undergo oligomerization and generate OM-IM fusion (Fig. 1C). The u-spanins have been proposed to be analogs of class II viral fusion proteins, partly based on the beta-sheet fold dominance. The pinholin-SAR endolysin system was also shown to require spanin-mediated OM disruption.

Analysis of 677 genomes of phages that infect Gram-negative bacteria hosts found that 586 encode identifiable spanins, with 528 having two-component spanins systems encoding separate i-spanin and o-spanin subunits, like λ, and 58 encode the unimolecular spanins, like phage T1 (2, 4). Interestingly, we were unable to identify spanins of either type within 91 genomes ("spaninless" phages), despite the ease of detecting signature features like the OM lipoprotein lipobox that is required in the genes of both o-spanins and u-spanins. Because OM disruption is required for lysis (3), we wondered if these phages used a different pathway. To address this question, we chose to examine the T7-like coliphage phiKT from the spaninless group. The results establish that some phages use an entirely different mode of OM disruption. The properties and function of the phiKT protein that effects this disruption, designated a "disruptin," are discussed in terms of a new model for the coordination of phage lysis.

RESULTS

phiKT gp28 complements a spanin defect in lambda lysis. phiKT is a virulent podophage of *E. coli* 4s that was isolated from horse feces (5). Like other members of the T7 superfamily, the late genes, including cistrons that are required for lysis, are arranged in tandem at the right end of the genome from ~16 kb onward. It should be noted that for the endolysin gene an incorrect downstream start codon had been chosen in the original GenBank submission (6). Once we made this correction, gp27 was identified as the endolysin based on its predicted soluble character and length (150 amino acids [aa]) and the residues Glu14-Cys23-Thr29 that match the canonical catalytic triad motif E-X_8-C/D-X_5-T, which is characteristic of the T4 endolysin family of glycoside hydrolases (7). Based on its proximity to the endolysin gene and the presence of four predicted transmembrane domains, gene 29 was annotated as the holin (127 aa, 13.2 kDa) (Fig. 1A). A rigorous manual analysis showed that there were no possible lipobox sequences in any of the remaining open reading frames (2). This absence rules out the presence of a putative spanin of either the unimolecular or two-component type because both involve a lipoprotein. Therefore, we considered whether phiKT infections ended in rapid lysis, as observed in all well-characterized dsDNA phages of

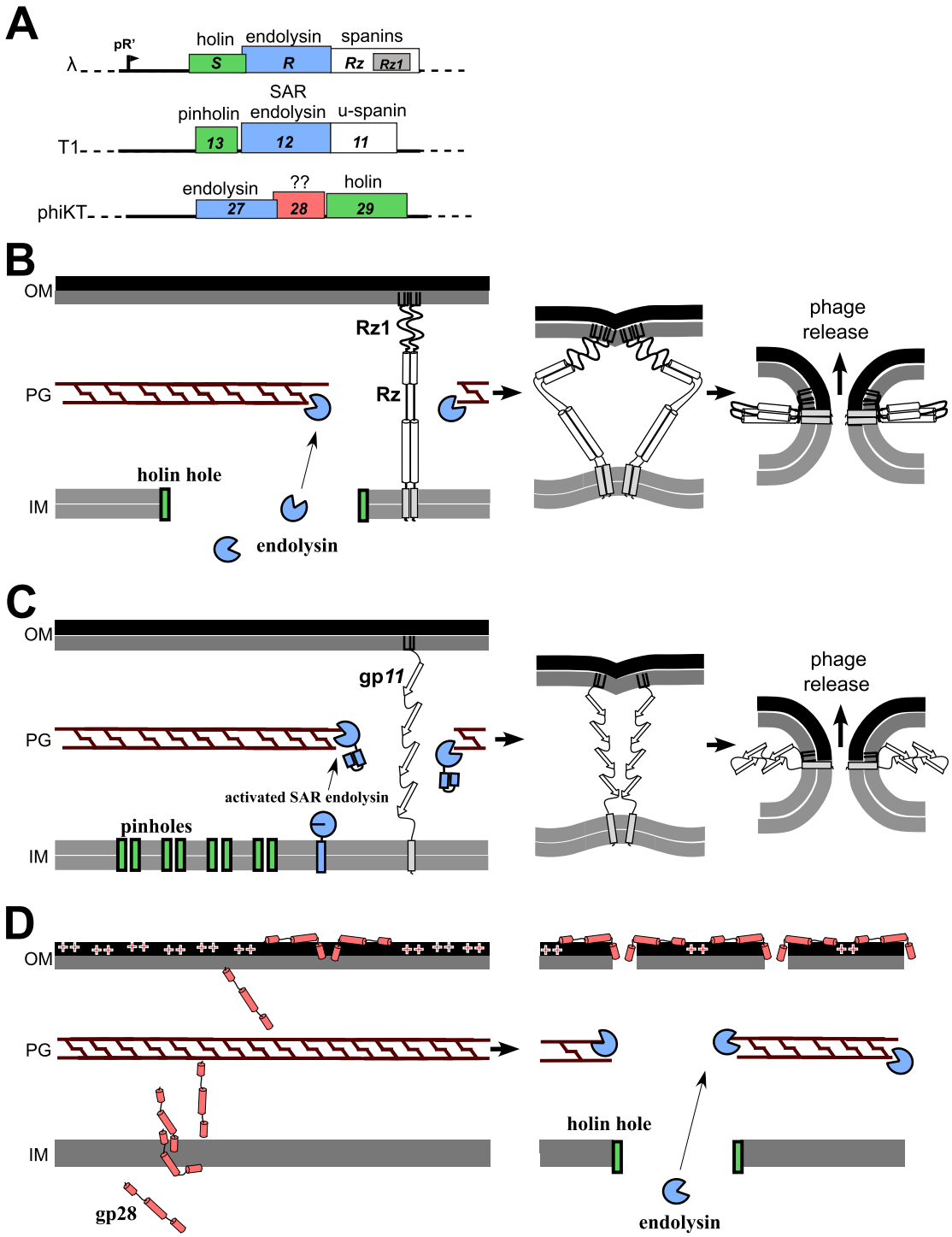

FIG 1 Phage use spanins or antimicrobial peptide-like small proteins to disrupt the OM during lysis. (A) Scaled comparisons of phage λ, T1, and phiKT lysis cassettes. λ lysis genes are expressed under pR′ promoter control and include a canonical large-hole holin, endolysin, and embedded two-component spanin (1). Phage T1 encodes a pinholin-SAR endolysin system with a unimolecular spanin (u-spanin). The lysis cassette of phiKT includes three genes encoding the putative endolysin (gene 27), a hypothetical novel protein that we designate as the disruptin (gene 28), and the putative holin (gene 29). (B) Two-component spanin (RzRz1) lysis as observed in phage λ proceeds as the holin breaches the IM, cytoplasmic endolysin reaches and degrades the PG, and spanins are freed to associate and fuse the IM and OM, effecting phage release. (C) With the unimolecular spanins, as in phage T1 lysis, the IM is compromised by a pinholin, which results in SAR endolysin release into the periplasm where it refolds and begins to degrade the PG. Finally, unimolecular spanins (gp11) allow phage escape when they fuse the IM and OM. (D) The disruptin model for lysis in phage phiKT differs from spanin lysis in that the gp28 molecules (red) are produced with the other lysis proteins and immediately positioned in both membranes before holin triggering. gp28 may displace cationic components stabilizing the LPS and simultaneously weakening the OM. After holin triggering and endolysin action, the weakened OM from gp28 displacement of cations results in cell lysis.

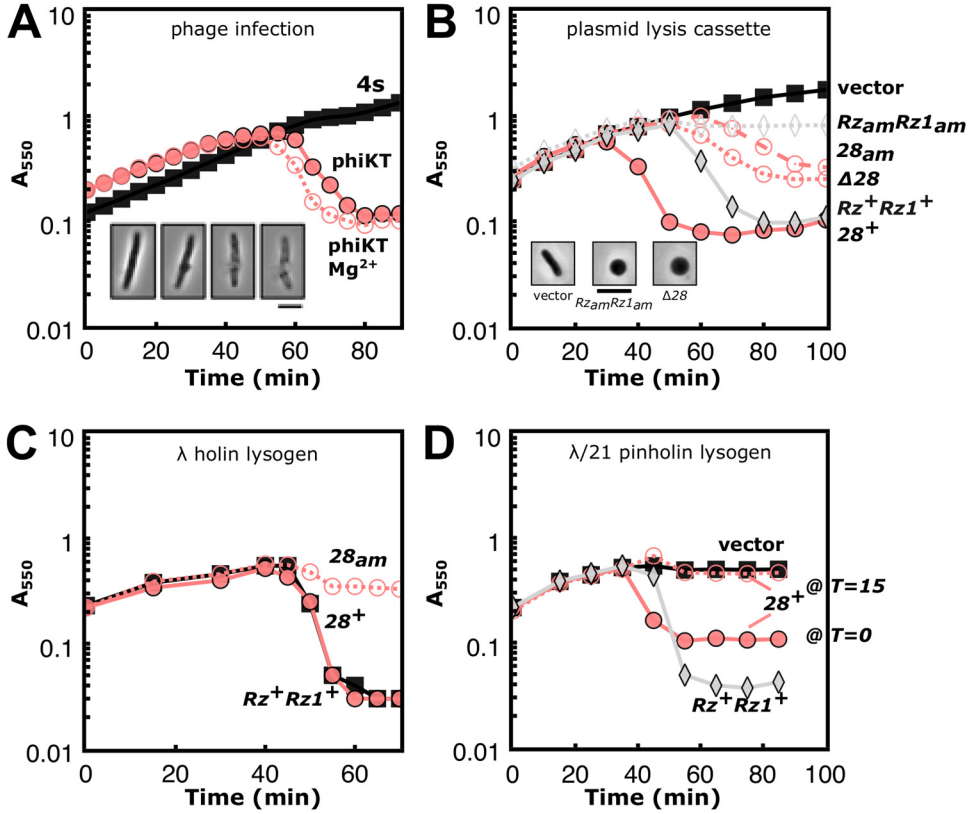

FIG 2 phiKT gp28 is necessary and sufficient for OM disruption during phage lysis. (A) *E. coli* 4s cultures (squares) were monitored for lysis after infection at $t = 0$ min with phiKT at an MOI of ~5 in the presence (open circles) or absence (filled circles) of 10 mM Mg^{2+} supplementation. (Inset) A single cell imaged at the time of lysis, with frames spanning approximately 1 s total (5 μm scale bar). (B) *E. coli* MG1655 cells carrying plasmids encoding full or partial phage lysis cassettes were induced by the addition of 1 mM IPTG at $t = 0$ min. Each construct carries the plasmid pQ, with lambda *Q* under *lacPO* control, and various derivatives of pRE, where lysis genes from phiKT or lambda are under the control of the lambda pR′ (Q-dependent) promoter. pRE inserts: none, squares ("vector"); phiKT *27-28-29*, filled circles ("28^{+}"); phiKT *27-Δ28-29*, open circles with dotted line ("*Δ28*"); *27-28*$_{E17X}$*-29*, open circles with dashed line ("28_{am}"); lambda *S105-R-Rz-Rz1*, filled diamonds ("$Rz^{+}Rz1^{+}$"); lambda *S105-R-Rz*$_{am}$*-Rz1*$_{am}$, open diamonds ("$Rz_{am}Rz1_{am}$"). A single cell imaged at $t = 60$ min is shown for vector, $Rz_{am}Rz1_{am}$, and *Δ28* with a 5 μm scale bar. (C) Cells carrying the spanin-defective prophage λ900 $Rz_{am}Rz1_{am}$, pQ, and various pRE constructs were induced by thermal induction and the addition of 1 mM IPTG at $t = 0$ min. The pRE plasmid constructs are labeled identically as in panel B. (D) Identical to panel C, including thermal induction at $t = 0$ min except the prophage is λ*hy21*(*SRRz*$_{am}$*Rz1*$_{am}$)^{21} and encodes the phage 21 pinholin and SAR endolysin. The "28^{+}" curves were induced for gp28 expression at $t = 0$ or 15 min, as indicated. All lysis curves were performed at least three times with similar results. A representative graph is shown.

Gram-negative hosts (3). Examination of phiKT infections in *E. coli* 4s revealed that the infection cycles terminated in a localized and catastrophic disruption of the cell, requiring approximately 1 s (Fig. 2A; see also Videos S1 and S2 in the supplemental material), indistinguishable from lytic events documented for coliphage lambda (3). Moreover, efficient lysis was observed irrespective of the presence of millimolar quantities of Mg^{2+} cations, which stabilize the fragile spherical cells that result from failed OM disruption in spanin mutant infections (3). We conclude that the OM is disrupted by phage-encoded lysis proteins during phiKT infections.

To identify these proteins, we searched for a segment of the phiKT genome that would encode all of the lysis gene functions. We previously established a two-plasmid system with the λ lysis cassette (Fig. 1A) that was cloned under its native late promoter on a medium copy number plasmid (pS105) and a second plasmid carrying the gene for the lambda late transcription factor Q under inducible control (pQ) (8, 9). Cells carrying these plasmids undergo saltatory lysis if induced during the logarithmic phase. Experiments with mutant alleles in each of the four lysis genes faithfully replicated the defective lysis phenotypes of the corresponding induced lysogens, including the

spherical cell phenotype for the null mutants of the spanin subunits (Fig. 2B) (3). Saltatory lysis was also obtained by inducing cells carrying pKT, a plasmid analogous to pS105 with the 27-28-29 gene cluster of phiKT replacing the lambda lysis genes. This indicated that these three genes constitute a complete lysis cassette (Fig. 2B). Moreover, if genes 27 and 29 encode the phiKT endolysin and holin, respectively, these results also suggest that gp28 fulfills the OM disruption function provided in lambda by the Rz/Rz1 spanin complex. To address this hypothesis, we created gene 28 null versions of plasmid pKT and tested them in the same induction system (Fig. 2B). Lysis was abrogated with both nonsense and deletion alleles. In addition, the terminal lysis-defective phenotype was spherical cells. Taken together, these results strongly indicate that the holin-endolysin (gp29 and gp27) system of phiKT achieves the degradation of the PG and that the role of gp28 is for OM disruption in phiKT lysis.

To determine whether this capacity for OM disruption was specific for the phiKT holin-endolysin system, we tested gp28 for its ability to complement the spanin lysis defect in lambda inductions (Fig. 2C). Lysogens carrying a $\lambda Rz_{am}Rz1_{am}$ prophage and plasmids with either RzRz1 or gene 28 under late promoter control were induced in the logarithmic phase and monitored for culture mass and cell morphology. Saltatory lysis was obtained for both constructs that was essentially indistinguishable in terms of kinetics and efficiency in the drop in optical density within bulk culture. We concluded that gp28 does not rely on a special feature of the phiKT lysis system and is fully capable of OM disruption even in the λ context.

The lambda R endolysin requires the nonspecific, micrometer-scale holes formed by the lambda holin to cross the IM and gain access to its PG target. This led us to investigate whether gp28 reaches the OM through large holin holes or if it crosses the IM by another mechanism. Notably, the phiKT endolysin gp27 is devoid of export signals, suggesting that the phiKT holin forms large holes to accommodate the endolysin. Furthermore, gp28 has no export signal that could account for transport to the OM by the characterized pathways. Therefore, we next asked whether it could function with the phage 21 pinholin-SAR endolysin system. The pinholin forms channels estimated at 2 nm or less (10), and these holes have been shown to be too small to permit release of soluble cytoplasmic proteins into the cytoplasm. Although culture lysis did not reach levels equal to spanin-mediated lysis, gp28 complements the spanin defect in the pinholin background when induced at t = 0 min, suggesting that large holin holes may facilitate its transport (Fig. 2D). Interestingly, when induced 15 min later, gp28 did not complement the spanin defect, which was likely because it had not accumulated to sufficient levels prior to the abrupt halt in protein synthesis caused by pinholin triggering. Because the pinholin holes are not large enough to support gp28 passage into the periplasm, these results strongly indicate that gp28 crosses the IM in a holin-independent fashion.

The gp28 disruptin is a cationic, membrane-associated, small protein. Because its primary structure rules out any mechanism requiring a periplasm-spanning complex that connects the IM and OM, as provided by the two-component and unimolecular spanins, we designated gp28 as the founding member of a new class of lysis proteins, the "disruptins". The 56-residue primary structure of gp28 is marked by a high fraction of charged residues (15 of 56 residues) that were predicted to be primarily helical with a net predicted charge of +7, where the basic residues were in clusters that could generate polar faces throughout the polypeptide (Fig. 3A). Because it is predicted to be a hydrophilic molecule and lacks any predicted membrane localization sequence yet functions to disrupt the OM, we assayed gp28 membrane localization.

First, we used a bulk membrane association test by fractionating lysed cells by the concerted action of lambda holin and endolysin paired with gp28 or the RzRz1 spanins into soluble and membrane fractions. The results showed that gp28 is quantitatively associated with the membrane fraction (Fig. 3B). Moreover, only a small fraction of gp28 can be removed from the membrane fraction by urea. Indeed, gp28 is resistant

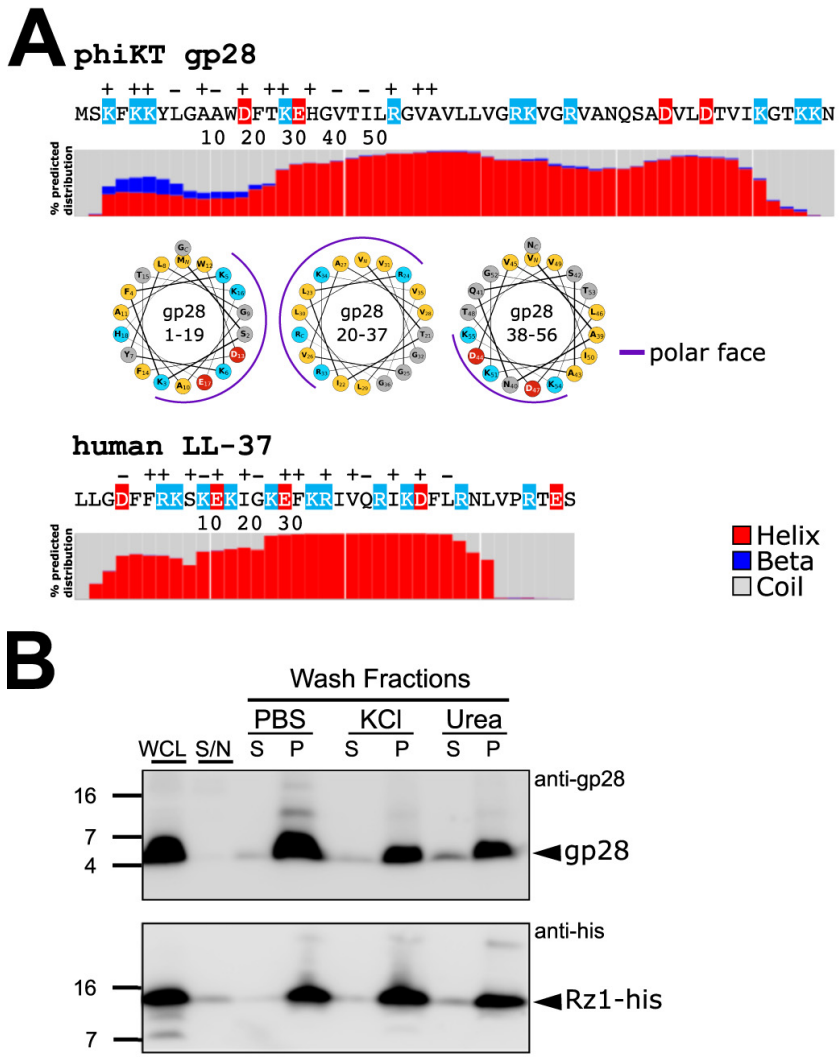

FIG 3 Hydrophobic interactions sequester gp28 in the membrane. (A) The 56-residue phiKT gp28 small protein and the human LL-37 peptide are shown residues with positively (blue) and negatively (red) charged residues highlighted. RaptorX-predicted secondary structure distributions are displayed below. A helical wheel projection of gp28 is displayed with polar faces marked. (B) Whole cell lysate (WCL) from MG1655 (λ900 $Rz_{am}Rz1_{am}$) cells with a pRE plasmid encoding the indicated protein were collected 55 min after induction and subjected to repeated ultracentrifugation steps to fractionate supernatant (S/N) from soluble (S) and insoluble pellet (P) proteins. Western blots of gp28 (top), and its control Rz1-His (bottom). Additionally, the pellet fraction was exposed to PBS, 2 M KCl or 6 M urea for solubilization before blotting where indicated.

to washing from the membrane-associated state like Rz1, which is a lipoprotein (Fig. 3B). These data confirm that gp28 is strongly associated with membranes.

Though the primary function of gp28 would require it to be at the OM, we hypothesized that gp28 would also associate with the IM, at least transiently, because it is synthesized in the cytosol. Because traditional methods of separating the IM and OM cannot be used on cells that have undergone holin-mediated lysis (11), we used immunofluorescence on fixed cells to visualize gp28 localization within cells. Furthermore, to distinguish between IM and OM localization, we performed plasmolysis treatment with a high sucrose buffer in which the IM retracts from the OM. Thus, IM proteins are contained within "plasmolysis bays" that are usually located at the cell pole(s) and can be identified within the brightfield or phase contrast image by a lighter cell region (12, 13). This was demonstrated with fluorescent fusions of known IM (Tar) and OM (OmpA) proteins, which display the expected localization patterns (Fig. 4A). Localization for gp28 expressed on a plasmid was assayed at 30 min when gp28 was expressed, but lysis would not have occurred. Without plasmolysis treatment, gp28

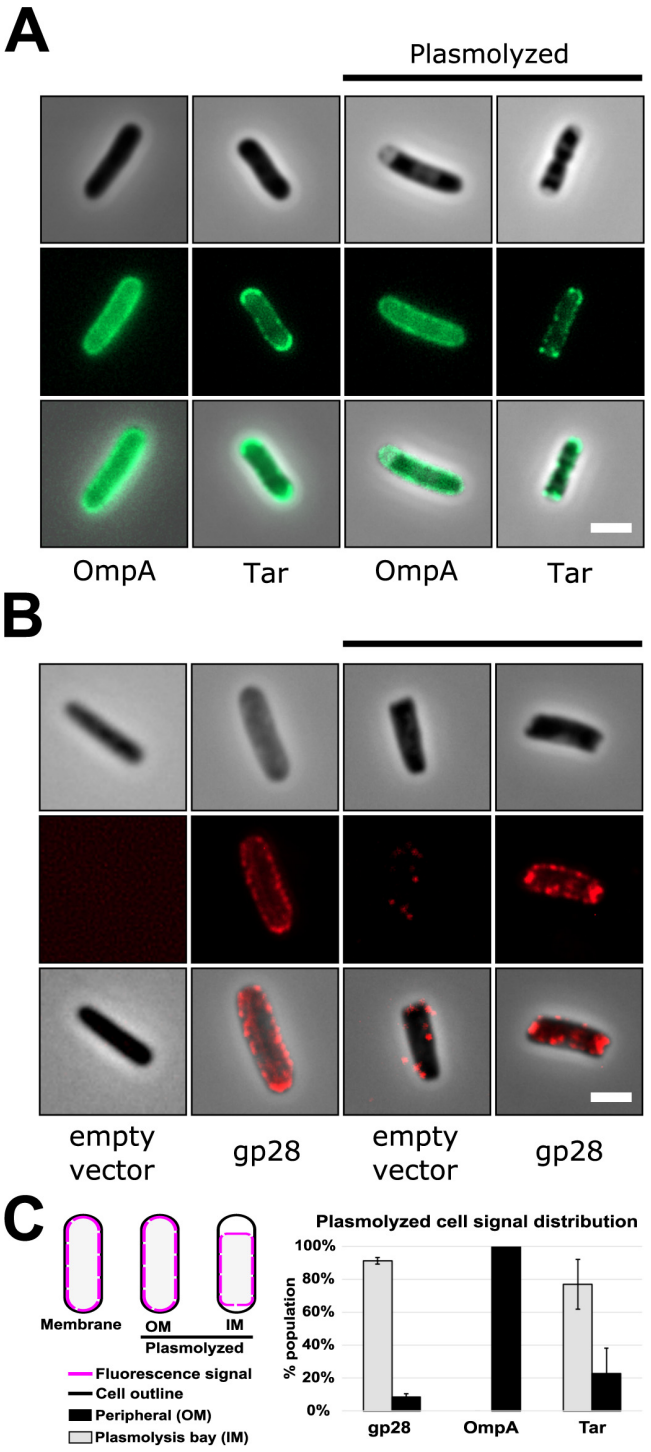

FIG 4 gp28 localizes to both the IM and OM. (A) Cells carrying OmpA-mNeon Green or Tar-GFP plasmids (see Materials and Methods) were induced and imaged live. Sucrose plasmolysis was applied to differentiate IM and OM localization (right panels). Representative images of single cells in brightfield, fluorescence and merged channels are shown. Scale bar is 2 μm. (B) MG1655 cells carrying pQ and pRE (28) were induced as in Fig. 2B at T = 0 min, fixed at 30 min, and analyzed by immunofluorescence microscopy using anti-gp*28* antibody. Left panels, no plasmolysis; right panels, plasmolysis with sucrose. Representative images for single cells are shown with a 2 μm scale bar. (C) Plasmolyzed cells were inspected for immunolocalization and categorized as OM (peripheral) or IM (plasmolysis bay) signal patterns ($n \geq 300$ per sample with standard deviation from at least 3 biological replicates).

had a peripheral localization pattern consistent with membrane proteins (Fig. 4B). In plasmolyzed cells, gp28 was associated primarily with the IM, although the OM localization pattern was also detectable (Fig. 4C). This result is consistent with a model where gp28 is embedded in the IM after synthesis and ultimately trafficked to the OM to exert its lytic function.

However, this led to another question; was gp28 capable of disrupting the IM? Given what we know about how holins control the timing of lysis and that having another lysis protein outside that regulation could be detrimental to a phage replication program, we expected that gp28 activity would be confined to the OM. To test this, we designed a fluorescence reporter assay where permeabilization of each membrane would be separately reported by ThT for the IM and Sytox for the OM (Fig. 5A). We verified using three cell backgrounds that the ThT dye only fluoresces when the IM is compromised. In cells where the holin was inactive (S_{am}) and neither membrane was compromised, no fluorescent signal was detected. In contrast, in cells where the holin had triggered destruction of the IM barrier, both with (round cells in $Rz_{am}Rz1_{am}$) and without (rods in R_{am}) PG degradation, there was a robust ThT signal (Fig. 5B). Under the conditions we tested, the Sytox signal was only observed with lysed cellular debris. Surprisingly, when we tested cells expressing gp28, we found that both membranes were permeable to these dyes with the signal for IM permeabilization becoming detectable before the signal for OM permeabilization (Fig. 5C). Additionally, using two alleles of gp28 that have distinct behavior from the wild-type (WT) native protein, we observed that the timing of permeabilization correlated with the lysis phenotype. For gp28 L46P, which is nonfunctional for OM disruption, the IM was permeabilized, but there was no signal for Sytox because the OM was never permeabilized. For gp28-His, which has a fast lysis phenotype, the OM permeabilization signal proportion was elevated and appeared earlier. Presumably, however, under its native expression during phage infection, gp28 did not attain levels sufficiently high to override the holin timed lysis control. We concluded that gp28 localizes to both the IM and OM and can disrupt the integrity of both membranes, perhaps in a concentration-dependent manner.

gp28 can function similarly to the cationic antimicrobial peptide LL-37. The defining characteristics and activity of gp28, including its small size, highly cationic primary structure, predominance of predicted alpha-helical character, membrane association, ability to cross membranes, and membrane-disrupting function, are the hallmarks of the cationic antimicrobial peptides (CAMPs). The human CAMP LL-37 (Fig. 3A) (14, 15) has been the subject of extensive studies in terms of its lethal interaction with bacterial cells, especially regarding its ability to cross both the OM and IM. LL-37, which is a small protein that is proteolytically processed when secreted (see Discussion), is 37 aa, has a +6 overall charge, and is largely alpha-helical. One way the CAMPs, as a class, are thought to disrupt the OM is by competing for binding sites for divalent cations in the lipopolysaccharide (LPS) (16, 17). To assess its capacity to act as a CAMP, we tested full-length synthetic gp28 in standard MIC and minimal bactericidal concentration (MBC) assays. The results showed that gp28 performed similarly to LL-37 against the native host for phiKT (4s) and the canonical laboratory *E. coli* strain (MG1655) (Fig. 6). These results indicated that gp28 is a phage-encoded antimicrobial peptide with similar activity to mammalian LL-37.

DISCUSSION

The first disruptin. OM disruption function is required for lysis by phage λ and is accomplished using its Rz/Rz1 two-component spanin system. The simplest hypothesis is that OM disruption is required for all phages of Gram-negative bacteria hosts. Here, we reported a new type of OM disruption protein, the disruptin, was identified for a coliphage, where we could rule out the presence of any clear lipoprotein gene and, thus, unimolecular or two-component spanins. This protein, phiKT gp28, fully complements the lysis defect associated with spanin absence in both the canonical holin-endolysin and pinholin-SAR endolysin systems. Remarkably, gp28 has many features that are hallmarks of CAMPs, like the well-studied human cathelicidin LL-37, including small size, a sequence that is rich in basic residues and dominated by predicted alpha-helical structure, and the ability to bind to and pass through the membranes. Moreover, synthetic gp28 exhibited antimicrobial activity comparable to LL-37 in standard MIC and MBC assays.

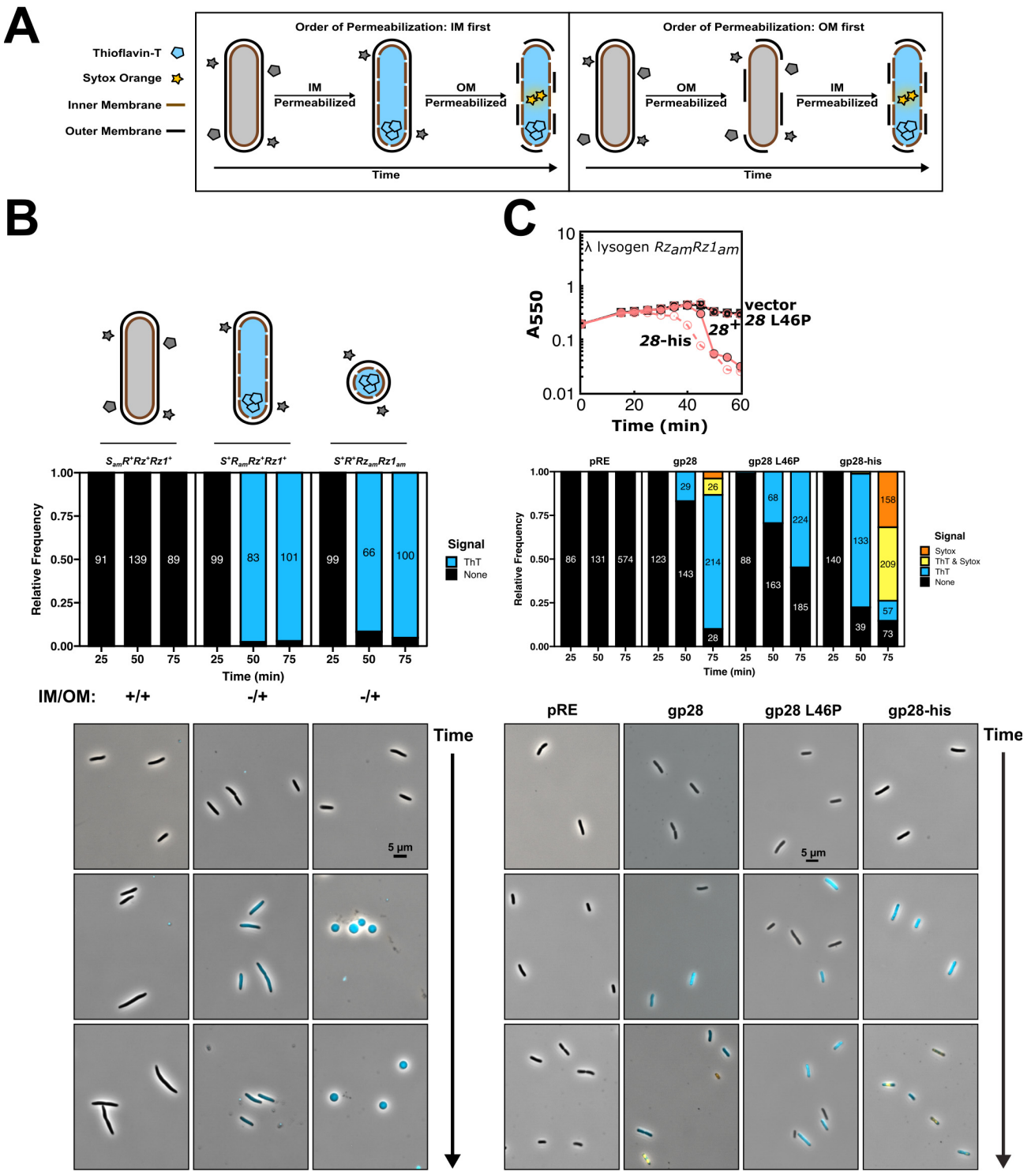

FIG 5 gp28 is capable of permeabilizing both the inner and outer membranes. (A) Experimental design for order of permeabilization experiments. The fluorescent DNA dyes ThT (OM permeable) and Sytox (membrane impermeable) were applied to cells and imaged over time to determine the order of membrane permeabilization. (B) MG1655 lysogens: λ900 S_{am}, λ900 R_{am}, or λ900 $Rz_{am}Rz1_{am}$ were used to validate the fluorescence assay at 25, 50, and 75 min postinduction. The quantification for each time point is graphed, where n = 72 to 139 cells were counted per sample with n_{total} = 883 cells, and representative images are shown. (C) For the lysis curve, cells carrying the spanin-defective prophage λ900 $Rz_{am}Rz1_{am}$ and various pRE constructs were induced by thermal induction and addition of 1 mM IPTG: none, squares ("vector"); gp28, filled circles ("*28*$^{+}$"); gp28-His, open circles with dashed line ("*28*-his"); gp*28* L46P, open circles with dotted line ("*28* L46P"). The permeability assay was applied to MG1655 cells carrying pQ and the empty pRE vector, or pRE with a gene 28 allele, including the native, L46P (nonfunctional), and His-tagged (hyperfunctional) forms. Three biological replicates were performed for each strain, except L46P which was measured in duplicate. In total, 2907 cells were quantified with 86 to 575 cells measured per sample. Representative images demonstrating the various signal patterns at each time are shown.

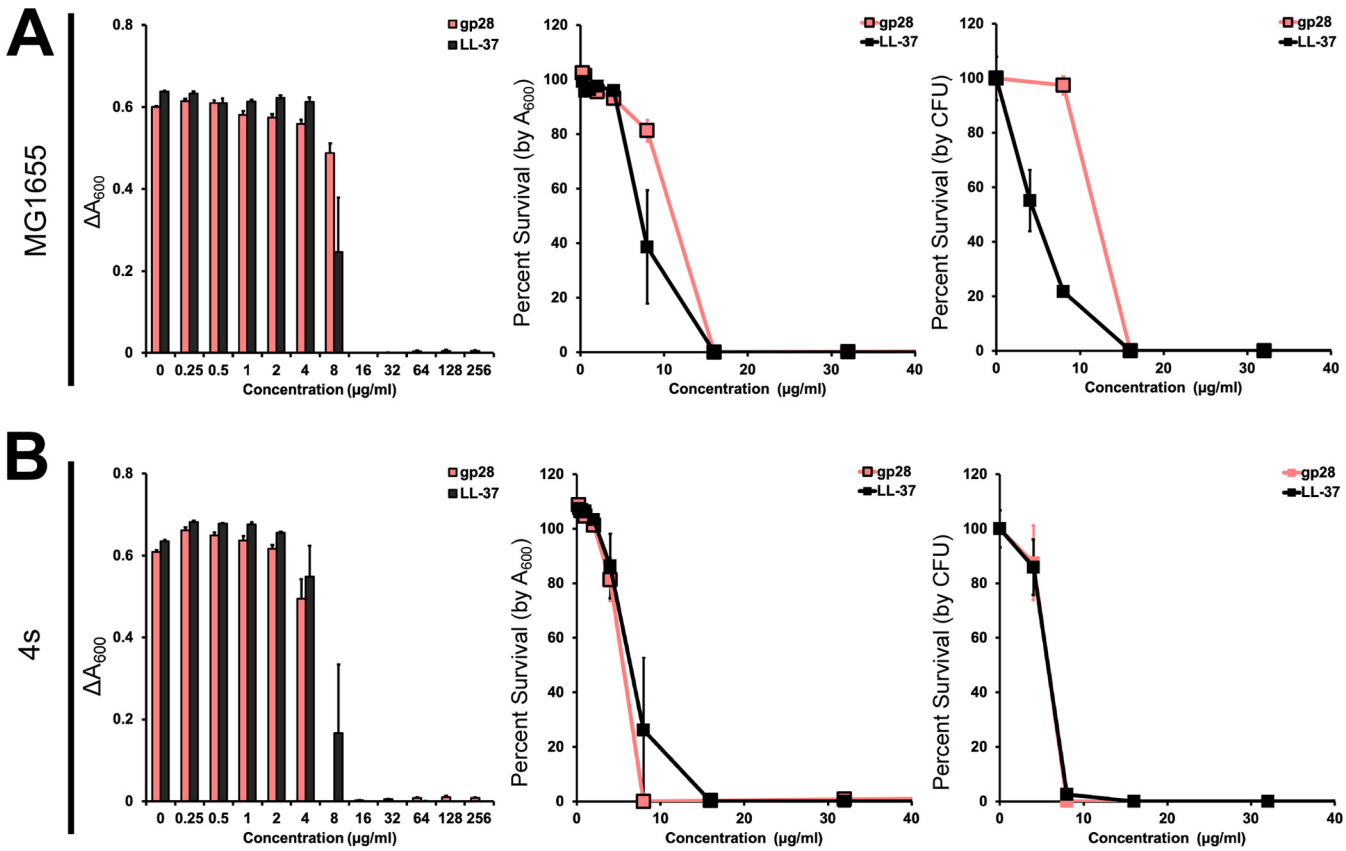

FIG 6 gp28 small protein displays antimicrobial properties. *E. coli* MG1655 (A) and 4s (B) strains were grown in standard MIC and minimum bactericidal concentration (MBC) conditions in 96-well plates. Bacteria were grown for 16 h in the presence of exogenously added synthetic gp28 and LL-37 peptide in 2-fold decreasing amounts for 16 h. The change in absorbance (A_{600}) and percent survival as a function of both absorbance and CFU/mL are plotted as a function of peptide concentration.

gp28 has no homologs in the NCBI nonredundant nucleotide database, except for a nearly identical protein in a closely related phage PGT2 (NCBI accession number ATS92463.1) (18). However, a previous report on the lysis system in *Pseudoalteromonas* phage PM2 found a small protein called P18 (formerly gpI) that may function like gp28 in the marine environment (19). The 51 aa P18 protein is highly charged. Although, in contrast to gp28, its charged residues are primarily positive in the N-terminal half and the latter half has negatively charged residues with an overall net charge of −1. However, similar to that of gp28, at least one-quarter of the total residues are charged. This protein is required for OM disruption, and an abrogating mutation in P18 results in fragile, round cells like that observed when spanins or the disruptin are absent. The authors also invoked a model whereby the effect of divalent cations stabilizing the OM must be overcome by the P18 protein, suggesting that a pore is formed. Additionally, several small proteins with similar sequences in other tailed phages were identified as potential paralogs.

We expect other spaninless phages that infect Gram-negative bacteria hosts also to encode disruptins with characteristics that match the CAMP or other AMP families. The task of identifying disruptins bioinformatically will be challenging, especially in uncharacterized or larger phage genomes with more than one predicted small, cationic, alpha-helical protein that may or may not be near other lysis genes. In a preliminary analysis of the 91 spaninless genomes, >500 candidates met an arbitrary cutoff of <80 aa and a minimum +4 net charge. Although choosing candidates in this way is noisy, the availability of the facile and rigorous RzRz1 complementation system used here makes this approach workable for single phage screening. Work along these lines is underway and could elucidate how general the disruptin solution is for OM destruction during phage lysis.

How does the disruptin function for OM disruption? gp28 was detected only in the particulate fractions, indicating that the gp28 protein has a strong affinity to membranes. Microscopy further revealed that the disruptin is also found in the OM even when expressed in the absence of other lysis proteins. The simplest notion is that, after synthesis in the cytosol, gp28 binds to the IM then passes through to the OM, where it becomes functional. The ability of gp28 to function with a pinholin system also supports this hypothesis. Both the preferential localization of gp28 to the OM and its OM disruption function may be explained by the ability of CAMPs to compete for the divalent cation binding sites in the LPS layer (16). Removal of a fraction of the stabilizing Mg^{2+}/Ca^{2+} ions resident in the phosphate-rich core LPS would likely reduce the tensile strength of the OM similar to that observed with EDTA treatment (20). Even a small reduction in the tensile strength of the OM would limit the load-bearing capacity required for resisting the turgor pressure at the last step of the lysis pathway. In other words, a weakened OM would be susceptible to rupture after endolysin-mediated destruction of the PG, which is the major contributor to cell envelope strength. It should be noted that, during the morphogenesis period, the disruptin should accumulate continuously in the OM and presumably destabilize it in terms of its barrier function with, presumably, negative consequences for the physiological health of the host cell. This may be one of the reasons why spanins are the dominant systems in phage lysis, i.e., the spanin systems have undetectable effects on host physiology until the encaging PG network is removed by the endolysin. As noted previously for holin function, the "all or nothing" character of phage lysis systems preserves the morphogenetic capacity of the host until the last possible instant before lysis (21).

Disruptin function in the context of holin control. Holins control the timing of lysis and, thus, the length and fecundity of the infection cycle (1). The timing is thought to reflect a characteristic mass-action property of holins, which accumulate harmlessly in the IM until reaching an allele-specific critical concentration and triggering lethal hole formation. This preserves the integrity of the IM and, thus, maximal biosynthetic capacity throughout the viral assembly phase of the infection cycle. Moreover, because single missense changes throughout the length of the holin can cause dramatic and unpredictable alteration of the critical concentration, a phage can rapidly evolve to sample drastically different infection cycle lengths (22–24). Theoretical and experimental analyses have suggested that environmental factors can favor shorter or longer infections, especially with respect to the average density of available hosts (25–28).

Both two-component and unimolecular spanin proteins accumulate in the envelope throughout the morphogenesis phase and, thus, are capable of subverting holin-mediated control of the lysis pathway. However, both types of spanins are blocked from a lethal function by being encaged in the meshwork of the PG, which in turn is maintained until the holin-controlled release of the endolysin. From this perspective, the use of the disruptin for the last step in the lysis pathway is surprising in that it prelocalizes to the IM and the OM irrespective of holin or endolysin function and offers no obvious feature that would confer subordination to holin control. Moreover, gp28 appears to have bactericidal capacity that is essentially indistinguishable from that of the well-studied CAMP LL-37. CAMPs are known to permeabilize both the IM and OM and cause a collapse of the proton motive force (PMF) (29–31). This seems even more problematic for the control of lysis timing because holins can be prematurely triggered even by partial reduction of the PMF (9). Indeed, comparing prophage inductions with gp28 and RzRz1 supplied in *trans* from a plasmid, where lysis begins earlier with the former, presumably reflecting earlier triggering of the pinholin but terminates at a higher residual optical density (Fig. 2D). The simplest interpretation is that gp28 had reached sufficient levels to impair the IM in many cells and, thus, trigger the holin without sufficient disruption of the OM. In support of this notion, delaying gp28 induction for 15 min resulted in a normal triggering by the pinholin, as reflected in the cessation of growth (Fig. 2D). In this scenario, gp28 did not achieve levels that poison the IM or destabilize the OM before the pinholin halts macromolecular synthesis.

The key to the compatibility of the disruptin with holin control likely resides in quantitative considerations. Membrane permeation typically requires binding of $>10^6$ CAMP molecules to the bacterial cell (32). However, the levels of expression of the lysis proteins in λ infections are on the order of 10^3 to 10^4 molecules at the time of lysis (33). Although the level of gp28 expression in phiKT infections has not yet been directly measured, it supports lysis when expressed from the λ late promoter under its native, unexceptional Shine-Dalgarno ribosome binding site (GGAGactttaATG). We suggest that, at the levels produced during the infection cycle, the disruptin neither affects the PMF as it binds and passes through the IM nor significantly permeabilizes the OM as it binds to the LPS and displaces a small fraction of the phosphate-neutralizing divalent cations. Accordingly, the effects of disruptin binding are not realized until the entire load of the cell turgor pressure is transferred to the OM by the endolysin-mediated degradation of the PG. To test this model, experiments using the noninvasive flagellum-tethered cells method can be used to quantify the PMF during gp28 expression (9, 34). In any case, it seems clear that holin or pinholin regulation of lysis timing is compatible with only a narrow window of disruptin gene expression. The evolutionary fitness cost may help explain why two-component and unimolecular spanin lysis systems are more abundant even though they require more genetic space, which is in short supply in many phages because of the packaging limits of the capsid.

The disruptin small protein as a CAMP. Nearly 20,000 antimicrobial peptides (AMPs) produced by eukaryotic and prokaryotic organisms have been documented and assembled into searchable databases primarily as an effort to find alternatives to antibiotics (for example, see references 35 to 37). The terminology, however, is misleading in that the AMPs produced by eukaryotes are small proteins that are synthesized as larger proprotein forms and secreted after proteolytic processing. In contrast, the AMPs produced by bacteria are often synthesized nonribosomally and become circular, branched, and/or populated with unusual amino acids and other moieties (38, 39). Among the most widespread and intensely studied, small, eukaryotic, antimicrobial proteins are the CAMPs (40), such as human cathelicidin LL-37, which was used here to gauge the AMP activity of gp28. CAMPs are extremely diverse but, in general, are small proteins with an overall basic charge dominated by a predicted alpha-helix conformation with strong amphipathic arrangement of polar and hydrophobic residues (15). All of these characteristics are shared by LL-37 and gp28. Several diverse mechanisms have been proposed for the bactericidal effects of CAMPs (17). These studies and other efforts to develop CAMPs for the clinic are hampered by the impracticality of implementing a genetic screen/selection system for determining the key residues involved in the interaction with the host envelope. They are difficult to express at high levels due to their toxicity in bacterial cells. In fact, much effort has been devoted to optimizing synthetic AMP design (39). gp28 may be a prototype to change the paradigm of CAMP structure-activity relationship studies, design, and modification. The enabling assumption is that, at the native levels of expression in phage infections, gp28 acts to weaken the OM and that this subverting interaction is the same one that confers bactericidal activity when added to the bacterial growth medium. By leveraging the disruptin requirement for lysis in the absence of spanin function, we suggest that phage and bacterial genetics could be used to optimize its effect on the OM and, thus, potentially improve its bactericidal capacity. For example, "plasmid-release", a technique developed in our laboratory, can be used to select for either enhanced or reduced OM damaging activity (41). In plasmid-release, plasmids encoding factors that accelerate or delay lysis can be enriched by recovering them from the medium or unlysed cells, respectively. Besides the obvious utility in the structure-function analysis of the disruptin, similar genetics-based approaches could be used to generate gp28 alleles with enhanced CAMP activity. Additionally, new disruptins may be isolated by using the same approach on metagenomic libraries from environmental samples, looking for genes encoding small proteins that would complement the spanin defect in *E. coli* or other bacteria in the future.

TABLE 1 Strains, phages, and plasmids

Name	Genotype and relevant features	Reference or source
Bacteriophages		
phiKT	Virulent podophage of *E. coli* 4s	5, 6
λ900	λΔ(*stf tfa*)::*cat* cI_{857} *bor*::*kan*, carries Cam^r and Kan^r	55
λ901 S_{am7}	λΔ(*stf tfa*)::*cat* cI_{857} *bor*::*kan* S_{am7}, which is S_{W56am}	Laboratory stock
λ900 R_{am}	λΔ(*stf tfa*)::*cat* cI_{857} *bor*::*kan* $R_{am54am60}$, which is the double amber allele $R_{Q26amW73am}$	Laboratory stock (56)
λ900 $Rz_{am}Rz1_{am}$	λΔ(*stf tfa*)::*cat* cI_{857} Rz_{Q100am} $Rz1_{W38am}$ *bor*::*kan*	55
Strains		
4s	Isolated from horse feces	5, 6
RY16390	MG1655 Δ*fhuA lacI*^{q} Δ*lacY*	Laboratory stock
MG1655 (λ900)	RY16390 lysogenized with λ900	Laboratory stock
MG1655 (λ900 S_{am7})	RY16390 lysogenized with λ900 S_{am7}	Laboratory stock
MG1655 (λ900 R_{am})	RY16390 lysogenized with λ900 R_{am}	Laboratory stock
MG1655 (λ900 $Rz_{am}Rz1_{am}$)	RY16390 lysogenized with λ900 $Rz_{am}Rz1_{am}$	Laboratory stock
MG1655 (λ900 hy21)	RY16390 lysogenized with λ900 hy(QSRRzRz1)21	57
Plasmids		
pRE	Medium copy plasmid containing Q-dependent λ late promoter pR′	58
pQ	λ Q cloned under $P_{lac/ara-1}$ promoter in a low copy no. plasmid pZS-24*	9
pRE seg 8	pRE containing phiKT lysis cassette (seg 8)	This study
pRE seg 8 $gp28_{E17X}$	pRE containing phiKT lysis cassette with a nonsense mutation at residue 17 of gene 28	This study
pRE seg 8 Δgp28	pRE containing phiKT lysis cassette with an in-frame deletion of residues 20 to 42 of gene 28	This study
pRE gp28	pRE containing phiKT gene 28	This study
pRE gp28-his	pRE containing phiKT gp28 with a C-terminal His tag	This study
pRE gp28 L46P	pRE containing phiKT gp28 with L46 changed to P	This study
pRE RzRz1	pRE containing λRzRz1	11
pRE Rz1-His	pRE containing λRz1 with His tag at the C-terminal end	11
pS105	*S105 R Rz Rz1* genes of λ cloned into pBR322	8
pS105 Rz_{am} $Rz1_{am}$	pS105 containing Rz_{Q100am} $Rz1_{W38am}$	59
pNM003	pTHV037-Ompa-SA1-177-(SA-1)-LEDPPAEL-mNeonGreenEColi	50
pBTar	pBAD18-Tar-GGSSAAG-GFP	Gift, Manson lab

MATERIALS AND METHODS

Strains, phages, plasmids, and primers. The strains, phages, and plasmids used in this study are presented in Table 1. The primers used for this study are summarized in Table 2 and were acquired from Integrated DNA Technologies (Coralville, IA, USA).

DNA manipulation. The pRE seg 8 plasmid was constructed by PCR amplifying the phiKT lysis cassette with the For phiKT seg 8 and Rev phiKT seg 8 primers. These primers contain KpnI and BamHI overhangs and were designed to amplify the section of the phiKT genome from nucleotide 36,581 to 37,741 (GenBank accession number NC_019520.1). The gel-purified PCR product was doubly digested with the corresponding restriction enzymes and ligated into pRE using T4 DNA ligase. The pRE gp28 plasmid was constructed by a similar method with the only modification being that the primers For gp28 and Rev gp28 were used to amplify from nucleotide 37067 to 37323 in the phiKT genome. QuikChange modifications were performed as described previously (42).

Bacterial growth, induction, and lysis monitoring. Bacterial cultures were grown, induced, and monitored for lysis as described previously (42). For phiKT infection, host *E. coli* 4s cultures were grown at 37°C to a in absorbance at 550 nm (A_{550}) of ~0.3. The cultures were put on ice, supplemented with

TABLE 2 Primers used in this study

Primer	Sequence (5′–3′)
For phiKT seg 8	AGTTCTGGTACCATGCTGATGCTGTGTCACCAT
Rev phiKT seg 8	GTCTACTGGATCCAGGCATCTAATCAGGGTCAGGT
For $gp28_{E17X}$	CACCAAGTAAACATGGTGTGACTATCCTGC
Rev $gp28_{E17X}$	CATGTTACTTGGTGAAATCCCATGCG
For gp28 deletion	CGCCGATGTACTTGATACGGT
Rev gp28 deletion	CCATGTTCCTTGGTGAAATCCCAT
For gp28	AGTTCTGGTACCGGCTGAATGCTCCGTATACACAAC
Rev gp28	GTCTACTGGATCCGTGGTCACAAGGGAACCGTAGTTC
For gp28 2	ACGGTCAGAGAGATTGATGTATGAGTAAATTCAAGAAATATCTGGGTG
Rev gp28-his	GTTATTGCTCAGACAGAAGCTTAAAGCTTCACCTTTAGCCACCGTG

$MgSO_4$ and $CaCl_2$ to a final level of 10 mM each, and infected with phage at a multiplicity of infection (MOI) of ~5. After 10 min, the cultures were again incubated at 37°C and monitored for lysis.

For thermal induction, lysogens were aerated at 30°C to an A_{550} of ~0.2, transferred for 15 min to 42°C to induce the prophage, and finally transferred to 37°C and monitored for lysis by A_{550} measurements. Cells carrying plasmids were grown at 37°C to A_{550} of ~0.2, then induced with 1 mM isopropyl-β-D-thiogalactopyranoside (IPTG) unless otherwise stated.

Phase contrast and fluorescence microscopy. A 1.5 μL culture sample was applied to a glass slide and covered with a coverslip. The sample was imaged immediately using a Zeiss Axio Observer 7 inverted microscope equipped with Plan-Apochromat 20×/0.8 numerical aperture (NA) Plan-Neofluar 40×/0.75 NA Ph2, and Alpha Plan-Apochromat 100×/1.46 oil (UV) Ph3 oil M27objectives, the Axiocam 702 mono camera, and the Colibri 7 LED light source. All image processing was done using the Zen 2.3 software.

Sequence analysis. The protein sequence for phiKT gp28 (NCBI accession number YP_007006611.1) and the processed form of the *Homo sapiens* antibacterial peptide LL-37 (NCBI accession number NP_004336.3) were retrieved for analysis. The charge profile was prepared in the Center for Phage Technology Galaxy instance using the Charges tool (43). Secondary structure predictions were performed using RaptorX (44, 45).

Bulk membrane association test. Growing cultures were induced at an A_{550} of 0.25 and 10 mL samples were collected 55 min after induction after the culture had cleared. Samples were placed on ice, and 1 μL of a protease inhibitor cocktail (Sigma-Aldrich, P8465) was added to each 10 mL sample. The treated lysate was centrifuged at 6,000 × *g* for 5 min at 4°C to clear unlysed cells. Three 3 mL aliquots of supernatant were taken from each 10 mL sample and centrifuged at 100,000 × *g* for 60 min at 4°C in a Beckman TLA-100.3 rotor in an Optima MAX-XP ultracentrifuge. After the centrifugation, the supernatant was removed, and the pellet was resuspended in 1× PBS, pH 7.4. A second centrifugation was performed at 100,000 × *g* as described above. Next, pellets were resuspended in 2 M KCl, 1× PBS, or 2 M urea. A final ultracentrifugation was carried out as above. After centrifugation, 1 mL of the supernatant and the pellet were collected for 10% trichloroacetic acid (TCA) precipitation, as previously described (46, 47). These TCA-precipitated samples were resuspended in nonreducing Laemmli buffer at 100 μL per 1 A_{550} unit (as measured at 40 min after induction of the original bulk culture). After boiling for 5 min, 30 μL of the samples were subjected to SDS-PAGE and Western blotting as described below.

SDS-PAGE and Western blotting. Samples were collected and prepared for Western blotting as described previously with reagents from Thermo Fisher (Waltham, MA) except where noted below (42). Prepared protein samples were resolved on a Novex 10 to 20% Tricine SDS-PAGE gel (Thermo Fisher Scientific). Gel transfer to 0.2 μm polyvinylidene difluoride (PVDF) and immunodetection were done using the iBlot and iBind systems (Invitrogen) according to the manufacturer's recommended protocol. The primary antibodies were diluted in 1× iBind solution at 1:2000, both rabbit anti-gp28 (Genscript, Piscataway, NJ, USA) and mouse anti-His for Rz1-His. Secondary antibodies were diluted 1:1000 in 1× iBind solution. Goat anti-mouse antibody–horseradish peroxidase (HRP; Thermo Scientific) developed with SuperSignal West Femto Maximum Sensitivity substrate and goat anti-rabbit antibody–HRP using SuperSignal West Pico PLUS were used for Rz1-His detection and gp28 detection, respectively. Chemiluminescence scanning was performed on an Amersham Imager 600 RGB (GE, Pittsburgh, PA) under default settings. Images were processed in LI-COR ImageStudioLite version 4.0.21 software.

Immunofluorescence localization. For cell preparation to perform immunofluorescence, protocols were adapted from references (48, 49). MG1655 *lacI*^{q} Δ*lacY* cells with pQ and pRE (or isogenic derivatives of pRE) were grown with aeration and the appropriate antibiotics at 37°C until reaching an A_{550} of ~0.2. The cultures were then induced with 1 mM IPTG. Thirty minutes later, cells were fixed for 15 min at room temperature by direct addition of premixed fixation reagents to the culture (18% formaldehyde, 0.3% glutaraldehyde, 41:1 ratio). Pelleted cells (5000 × *g* for 5 min at room temperature) were gently washed three times in 1× PBS at pH 7.4 and stored at 4°C for up to 1 week. Other cells prepared under identical conditions were pelleted, then treated with high solute buffer (15% sucrose, 25 mM Tris, pH 7.5) for 15 min to induce plasmolysis. After a quick PBS wash, these cells were subjected to fixation.

Before staining, fixed cells were permeabilized by resuspension in 0.1% Triton X-100, 10 mM EDTA, and 100 μg/mL lysozyme for 25 min at room temperature. Cells were blocked in 2% bovine serum albumin (BSA) at room temperature for 20 min followed by incubation with preabsorbed anti-gp28 diluted 1:200 in 2% BSA for 1 h at 4°C. The secondary antibody AF647 (Invitrogen AF3273) was diluted to a 5 μg/mL final concentration (1:400) in 2% BSA and incubated for 1 h in the dark at 4°C. After 3 to 6 washes in PBS, the samples were imaged immediately or stored at 4°C until imaging.

To validate IM and OM localization, plasmids carrying inducible genes for the OM fusion OmpA-mNeonGreen (pTHV037-Ompa-SA1-177-(SA-1)-LEDPPAEL-mNGEC or pNM003) or the IM fusion Tar-GFP (pBTar, pBAD18-Tar-GGSSAAG-GFP) were grown in LB, induced, and imaged live (50). The OmpA and Tar constructs were both induced at an A_{550} of ~0.2. The former was grown at 30°C and induced with 15 μM IPTG according to the previously published method (50). The latter was grown at 37°C and induced with 0.002% arabinose. To visualize, both antibody-labeled and fluorescent cells were added to glass slides with coverslips and imaged on a Zeiss Axio Observer 7 inverted microscope using an Alpha Plan-Apochromat 100×/1.46 oil (UV) Ph3 M27-oil objective. Z-stacks for the fluorescent channel were deconvoluted using the Zen 2.3 software.

Permeabilization assay with ThT and Sytox Orange. Thioflavin-T (ThT) was purchased from Sigma-Aldrich (St. Louis, MO). Stocks were made in filter-sterilized water and kept at −20°C before use. Sytox Orange was purchased from Thermo Fisher Scientific (Waltham, MA). Stocks were made in filter-sterilized water at 100 μM and kept at −20°C before use. Before use, Sytox Orange was diluted 1:100 in sterile Milli-Q water to a concentration of 1 μM. ThT and Sytox Orange were used in LB at final concentrations of 10 μM and 0.1 μM, respectively.

For the controls, MG1655 lysogens were grown and induced by a temperature shift as described above. For the plasmid-based expression, MG1655 *lacI*^{q} Δ*lacY* cells carrying the pQ and pRE plasmids (or derivatives) were induced with 1 mM IPTG. At times before, during, and after holin triggering, 89 μL samples were collected for imaging and stained with dye mix then imaged immediately with both fluorescent channel exposures set to 125 ms.

MIC and minimal bactericidal concentration (MBC_{99}) of peptides gp28 and LL-37. Synthetic gp28 (Genscript USA, Piscataway, NJ) and LL-37 peptides were dissolved in double-distilled H_2O to give a stock concentration of 5.12 mg/mL and aliquots were stored at −80°C. The maximum concentration of peptides used for the assays was 256 μg/mL. For each assay, primary cultures of *E. coli* MG1655 or 4s were started from a −80°C stock and grown overnight in Mueller-Hinton (MH) medium at 37°C shaking. A secondary culture started in the late logarithmic phase (A_{600} of ~1.5 to 2) was used to prepare the starting inoculum in MH media with 0.001% acetic acid and 0.02% BSA, diluted to give an A_{600} of ~0.001, which corresponded to ~5×10^5 colony forming units (CFU) per milliliter of bacteria. Using 96-well polypropylene, nonpyrogenic cell culture plates (Corning Incorporated, Corning, NY), 100 μL of 5×10^5 CFU/mL bacteria were added in triplicate for each peptide. Each antimicrobial agent was assayed at 11 different concentrations from 2-fold serial dilutions. Plates were incubated in a humidity-controlled incubator at 37°C for 16 h. A_{600} was measured using a PerkinElmer Envision 2104 multilabel plate reader (Perkin Elmer, Waltham, MA) at the start of the assay and at 16 h. After 16 h, bacteria were plated for CFU counts on MH agar plates. Percent survival was determined for each peptide concentration using A_{600} and CFU per milliliter compared to the untreated sample at 16 h. The MIC and MBC_{99} values were calculated relative to the starting CFU per milliliter. MIC was defined as the minimal concentration of the peptide needed to inhibit the growth of the starting culture of bacteria (≤100%). MBC_{99} was defined as the minimal concentration of the peptide needed to kill 99% of the starting culture of bacteria (≤1%). These assays were done in triplicate.

Figure preparation. Data were graphed using either R 4.0.4 with ggplot2 3.3.3, ggprism 1.0.2, and dpylr 1.0.5 (51–54) or using Plotly (Plotly Technologies Inc., Montréal, QC). Graphics for figures were combined for display in Inkscape 1.0 (https://inkscape.org/).

SUPPLEMENTAL MATERIAL

Supplemental material is available online only.

SUPPLEMENTAL FILE 1, AVI file, 0.4 MB.

SUPPLEMENTAL FILE 2, AVI file, 0.2 MB.

SUPPLEMENTAL FILE 3, PDF file, 0.01 MB.

ACKNOWLEDGMENTS

This work was supported by grant numbers GM27099, GM136396, and AI149383 from the Public Health Service, grant number HRD-1304975 from the National Science Foundation, two Beckman Scholars Program Awards from the Arnold and Mabel Beckman Foundation, and the Center for Phage Technology at Texas A&M University, which is jointly sponsored by Texas A&M AgriLife. The funders had no role in study design, data collection, and interpretation, or the decision to submit the work for publication. We thank the Young lab members, past and present, for their valuable input during this study. Daisy Wilbert provided excellent clerical support. Jacob Chamblee wrote the Python code used for graphing with Plotly. The phage phiKT and its 4s host strain were generous gifts from Andrey Letarov and Petr Leiman of the Russian Academy of Sciences, Moscow, Russia. The pNM003 OmpA plasmid was a gift from Tanneke den Blaauwen at University of Amsterdam. The pBTar plasmid was a gift from Michael Manson at Texas A&M University. The Sytox reagent was a generous gift from Jennifer Herman and Matthew Theodore at Texas A&M University. The authors also acknowledge the efforts expended by Kelsey Bettridge, Ryan McQuillen, and Jie Xiao at John Hopkins University for use of the super resolution microscopy for gp28 localization in initial experiments that were ultimately not included in this report, although some were in a preprint version of this work.

Author contributions according to the CRediT taxonomy: A.H., J.C., and R.Y. Conceptualization; A.H., J.C., J.R., and C.M. Data Curation; R.Y. Funding Acquisition; A.H., J.C., J.R., C.M., C.O., R.M., L.T.M., T.G., R.S., P.S., and R.Y. Investigation; J.C. Methodology; J.C., J.R., and R.Y. Project Administration; J.C., J.D.C., and R.Y. Resources; J.C., J.R., and J.D.C. Supervision; A.H., J.C., J.R., C.M., C.O., R.M., L.T.M. Validation; J.C., J.R., C.M., Visualization; J.C., J.R., and R.Y. Writing – original draft; A.H., J.C., J.R., C.M., C.O., R.M., L.T.M., T.G., R.S., P.S., J.D.C., and R.Y. Writing – review & editing.

We declare no conflict of interest.

REFERENCES

1. Cahill J, Young R. 2019. Phage lysis: multiple genes for multiple barriers. Adv Virus Res 103:33–70. https://doi.org/10.1016/bs.aivir.2018.09.003.
2. Kongari R, Rajaure M, Cahill J, Rasche E, Mijalis E, Berry J, Young R. 2018. Phage spanins: diversity, topological dynamics and gene convergence. BMC Bioinformatics 19:326. https://doi.org/10.1186/s12859-018-2342-8.
3. Berry J, Rajaure M, Pang T, Young R. 2012. The spanin complex is essential for lambda lysis. J Bacteriol 194:5667–5674. https://doi.org/10.1128/JB.01245-12.
4. Summer EJ, Berry J, Tran TAT, Niu L, Struck DK, Young R. 2007. Rz/Rz1 lysis gene equivalents in phages of Gram-negative hosts. J Mol Biol 373:1098–1112. https://doi.org/10.1016/j.jmb.2007.08.045.
5. Knirel YA, Prokhorov NS, Shashkov AS, Ovchinnikova OG, Zdorovenko EL, Liu B, Kostryukova ES, Larin AK, Golomidova AK, Letarov AV. 2015. Variations in O-antigen biosynthesis and O-acetylation associated with altered phage sensitivity in *Escherichia coli* 4s. J Bacteriol 197:905–912. https://doi.org/10.1128/JB.02398-14.
6. Golomidova A, Kulikov E, Isaeva A, Manykin A, Letarov A. 2007. The diversity of coliphages and coliforms in horse feces reveals a complex pattern of ecological interactions. Appl Environ Microbiol 73:5975–5981. https://doi.org/10.1128/AEM.01145-07.
7. Kuroki R, Weaver L, Matthews B. 1993. A covalent enzyme-substrate intermediate with saccharide distortion in a mutant T4 lysozyme. Science 262:2030–2033. https://doi.org/10.1126/science.8266098.
8. Smith DL, Struck DK, Scholtz JM, Young R. 1998. Purification and biochemical characterization of the lambda holin. J Bacteriol 180:2531–2540. https://doi.org/10.1128/JB.180.9.2531-2540.1998.
9. Gründling A, Manson MD, Young R. 2001. Holins kill without warning. Proc Natl Acad Sci U S A 98:9348–9352. https://doi.org/10.1073/pnas.151247598.
10. Pang T, Savva CG, Fleming KG, Struck DK, Young R. 2009. Structure of the lethal phage pinhole. Proc Natl Acad Sci U S A 106:18966–18971. https://doi.org/10.1073/pnas.0907941106.
11. Berry J, Summer EJ, Struck DK, Young R. 2008. The final step in the phage infection cycle: the Rz and Rz1 lysis proteins link the inner and outer membranes. Mol Microbiol 70:341–351. https://doi.org/10.1111/j.1365-2958.2008.06408.x.
12. Fishov I, Woldringh CL. 1999. Visualization of membrane domains in *Escherichia coli*. Mol Microbiol 32:1166–1172. https://doi.org/10.1046/j.1365-2958.1999.01425.x.
13. Boy D, Koch H-G. 2009. Visualization of distinct entities of the SecYEG translocon during translocation and integration of bacterial proteins. Mol Biol Cell 20:1804–1815. https://doi.org/10.1091/mbc.e08-08-0886.
14. Turner J, Cho Y, Dinh N-N, Waring AJ, Lehrer RI. 1998. Activities of LL-37, a cathelin-associated antimicrobial peptide of human neutrophils. Antimicrob Agents Chemother 42:2206–2214. https://doi.org/10.1128/AAC.42.9.2206.
15. Xhindoli D, Pacor S, Benincasa M, Scocchi M, Gennaro R, Tossi A. 2016. The human cathelicidin LL-37 - a pore-forming antibacterial peptide and host-cell modulator. Biochim Biophys Acta 1858:546–566. https://doi.org/10.1016/j.bbamem.2015.11.003.
16. Ebbensgaard A, Mordhorst H, Aarestrup FM, Hansen EB. 2018. The role of outer membrane proteins and lipopolysaccharides for the sensitivity of *Escherichia coli* to antimicrobial peptides. Front Microbiol 9:2153. https://doi.org/10.3389/fmicb.2018.02153.
17. Huang Y, Huang J, Chen Y. 2010. Alpha-helical cationic antimicrobial peptides: relationships of structure and function. Protein Cell 1:143–152. https://doi.org/10.1007/s13238-010-0004-3.
18. Golomidova AK, Kulikov EE, Kudryavtseva AV, Letarov AV. 2018. Complete genome sequence of *Escherichia coli* bacteriophage PGT2. Genome Announc 6:31. https://doi.org/10.1128/genomeA.01370-17.
19. Krupovic M, Daugelavicius R, Bamford DH. 2007. A novel lysis system in PM2, a lipid-containing marine double-stranded DNA bacteriophage. Mol Microbiol 64:1635–1648. https://doi.org/10.1111/j.1365-2958.2007.05769.x.
20. Leive L. 1974. The barrier function of the gram-negative envelope. Ann N Y Acad Sci 235:109–129. https://doi.org/10.1111/j.1749-6632.1974.tb43261.x.
21. Young R. 1992. Bacteriophage lysis: mechanism and regulation. Microbiol Rev 56:430–481. https://doi.org/10.1128/mr.56.3.430-481.1992.
22. Raab R, Neal G, Sohaskey C, Smith J, Young R. 1988. Dominance in lambda S mutations and evidence for translational control. J Mol Biol 199:95–105. https://doi.org/10.1016/0022-2836(88)90381-6.
23. Johnson-Boaz R, Chang CY, Young R. 1994. A dominant mutation in the bacteriophage lambda S gene causes premature lysis and an absolute defective plating phenotype. Mol Microbiol 13:495–504. https://doi.org/10.1111/j.1365-2958.1994.tb00444.x.
24. Zheng Y, Struck DK, Dankenbring CA, Young R. 2008. Evolutionary dominance of holin lysis systems derives from superior genetic malleability. Microbiology (Reading) 154:1710–1718. https://doi.org/10.1099/mic.0.2008/016956-0.
25. Wang I-N. 2006. Lysis timing and bacteriophage fitness. Genetics 172:17–26. https://doi.org/10.1534/genetics.105.045922.
26. Bull JJ, Pfennig DW, Wang I-N. 2004. Genetic details, optimization and phage life histories. Trends Ecol Evol 19:76–82. https://doi.org/10.1016/j.tree.2003.10.008.
27. Abedon ST, Hyman P, Thomas C. 2003. Experimental examination of bacteriophage latent-period evolution as a response to bacterial availability. Appl Environ Microbiol 69:7499–7506. https://doi.org/10.1128/AEM.69.12.7499-7506.2003.
28. Wang I-N, Dykhuizen DE, Slobodkin LB. 1996. The evolution of phage lysis timing. Evol Ecol 10:545–558. https://doi.org/10.1007/BF01237884.
29. Choi H, Rangarajan N, Weisshaar JC. 2016. Lights, Camera, Action! Antimicrobial Peptide Mechanisms Imaged in Space and Time. Trends Microbiol 24:111–122. https://doi.org/10.1016/j.tim.2015.11.004.
30. Nguyen LT, Haney EF, Vogel HJ. 2011. The expanding scope of antimicrobial peptide structures and their modes of action. Trends Biotechnol 29:464–472. https://doi.org/10.1016/j.tibtech.2011.05.001.
31. Tossi A, Sandri L, Giangaspero A. 2000. Amphipathic, α-helical antimicrobial peptides. Peptide Sci 55:4–30. https://doi.org/10.1002/1097-0282(2000)55:1<4::AID-BIP30>3.0.CO;2-M.
32. Roversi D, Luca V, Aureli S, Park Y, Mangoni ML, Stella L. 2014. How many antimicrobial peptide molecules kill a bacterium? The case of PMAP-23. ACS Chem Biol 9:2003–2007. https://doi.org/10.1021/cb500426r.
33. White R, Chiba S, Pang T, Dewey JS, Savva CG, Holzenburg A, Pogliano K, Young R. 2011. Holin triggering in real time. Proc Natl Acad Sci U S A 108:798–803. https://doi.org/10.1073/pnas.1011921108.
34. Manson MD, Tedesco PM, Berg HC. 1980. Energetics of flagellar rotation in bacteria. J Mol Biol 138:541–561. https://doi.org/10.1016/s0022-2836(80)80017-9.
35. Piotto SP, Sessa L, Concilio S, Iannelli P. 2012. YADAMP: yet another database of antimicrobial peptides. Int J Antimicrob Agents 39:346–351. https://doi.org/10.1016/j.ijantimicag.2011.12.003.
36. Kang X, Dong F, Shi C, Liu S, Sun J, Chen J, Li H, Xu H, Lao X, Zheng H. 2019. DRAMP 2.0, an updated data repository of antimicrobial peptides. Sci Data 6:148. https://doi.org/10.1038/s41597-019-0154-y.
37. Wang G, Li X, Wang Z. 2016. APD3: the antimicrobial peptide database as a tool for research and education. Nucleic Acids Res 44:D1087–93. https://doi.org/10.1093/nar/gkv1278.
38. Hassan M, Kjos M, Nes IF, Diep DB, Lotfipour F. 2012. Natural antimicrobial peptides from bacteria: characteristics and potential applications to fight against antibiotic resistance. J Appl Microbiol 113:723–736. https://doi.org/10.1111/j.1365-2672.2012.05338.x.
39. Sarkar T, Chetia M, Chatterjee S. 2021. Antimicrobial peptides and proteins: from nature's reservoir to the laboratory and beyond. Front Chem 9:691532. https://doi.org/10.3389/fchem.2021.691532.
40. Boparai JK, Sharma PK. 2020. Mini review on antimicrobial peptides, sources, mechanism and recent applications. Protein Pept Lett 27:4–16. https://doi.org/10.2174/0929866526666190822165812.
41. Chamakura KR, Sham L-T, Davis RM, Min L, Cho H, Ruiz N, Bernhardt TG, Young R. 2017. A viral protein antibiotic inhibits lipid II flippase activity. Nat Microbiol 2:1480–1484. https://doi.org/10.1038/s41564-017-0023-4.
42. Cahill J, Rajaure M, Holt A, Moreland R, O'Leary C, Kulkarni A, Sloan J, Young R. 2017. Suppressor analysis of the fusogenic lambda spanins. J Virol 91:e00413-17. https://doi.org/10.1128/JVI.00413-17.
43. Ramsey J, Rasche H, Maughmer C, Criscione A, Mijalis E, Liu M, Hu JC, Young R, Gill JJ. 2020. Galaxy and Apollo as a biologist-friendly interface for high-quality cooperative phage genome annotation. PLoS Comput Biol 16:e1008214. https://doi.org/10.1371/journal.pcbi.1008214.
44. Wang S, Li W, Liu S, Xu J. 2016. RaptorX-Property: a web server for protein structure property prediction. Nucleic Acids Res 44:W430–W435. https://doi.org/10.1093/nar/gkw306.
45. Källberg M, Wang H, Wang S, Peng J, Wang Z, Lu H, Xu J. 2012. Template-based protein structure modeling using the RaptorX web server. Nat Protoc 7:1511–1522. https://doi.org/10.1038/nprot.2012.085.
46. Berry JD, Rajaure M, Young R. 2013. Spanin function requires subunit homodimerization through intermolecular disulfide bonds. Mol Microbiol 88:35–47. https://doi.org/10.1111/mmi.12167.

47. Berry J, Savva C, Holzenburg A, Young R. 2010. The lambda spanin components Rz and Rz1 undergo tertiary and quaternary rearrangements upon complex formation. Protein Sci 19:1967–1977. https://doi.org/10.1002/pro.485.
48. Buddelmeijer N, Aarsman M, den Blaauwen T. 2013. Immunolabeling of proteins in situ in *Escherichia coli* K12 strains. Bio-protocol 3:e852. https://doi.org/10.21769/BioProtoc.852.
49. Webb CT, Selkrig J, Perry AJ, Noinaj N, Buchanan SK, Lithgow T. 2012. Dynamic association of BAM complex modules includes surface exposure of the lipoprotein BamC. J Mol Biol 422:545–555. https://doi.org/10.1016/j.jmb.2012.05.035.
50. Meiresonne NY, van derPloeg R, Hink MA, den Blaauwen T. 2017. Activity-related conformational changes in d,d-carboxypeptidases revealed by in vivo periplasmic Förster Resonance Energy Transfer assay in *Escherichia coli*. mBio 8:e01089-17. https://doi.org/10.1128/mBio.01089-17.
51. R Core Team. 2021. R: A Language and Environment for Statistical Computing. https://www.R-project.org. Retrieved 15 Feb 2021.
52. Wickham H. 2016. ggplot2: elegant graphics for data analysis. Springer-Verlag New York. https://ggplot2.tidyverse.org.
53. Wickham H, François R, Henry L, Müller K, RStudio. 2021. dplyr: a grammar of data manipulation. https://CRAN.R-project.org/package=dplyr. Retrieved 5 March 2021.
54. Dawson C. 2021. ggprism: A 'ggplot2' extension inspired by GraphPad Prism. https://CRAN.R-project.org/package=ggprism. Retrieved 22 Feb 2021.
55. Zhang N, Young R. 1999. Complementation and characterization of the nested Rz and Rz1 reading frames in the genome of bacteriophage lambda. Mol Gen Genet 262:659–667. https://doi.org/10.1007/s004380051128.
56. Cahill JL. 2017. Molecular, genetic, and biochemical analysis of phage lambda lysis.
57. Barenboim M, Chang CY, Dib Hajj F, Young R. 1999. Characterization of the dual start motif of a class II holin gene. Mol Microbiol 32:715–727. https://doi.org/10.1046/j.1365-2958.1999.01385.x.
58. Park T, Struck DK, Deaton JF, Young R. 2006. Topological dynamics of holins in programmed bacterial lysis. Proc Natl Acad Sci U S A 103:19713–19718. https://doi.org/10.1073/pnas.0600943103.
59. White R, Tran TAT, Dankenbring CA, Deaton J, Young R. 2010. The N-terminal transmembrane domain of λ S is required for holin but not antiholin function. J Bacteriol 192:725–733. https://doi.org/10.1128/JB.01263-09.